Chemical Physics 522 (2019) 24–31

Contents lists available at ScienceDirect

Chemical Physics

journal homepage: www.elsevier.com/locate/chemphys

Insight into the diffusion mechanism of Cu cluster over Cu(111) surface: Effect of syngas and H_2S atmosphere on Cu diffusion

Xiaobin Hao, Riguang Zhang*, Lixia Ling, Baojun Wang*

Key Laboratory of Coal Science and Technology of Ministry of Education and Shanxi Province, Taiyuan University of Technology, Taiyuan 030024, Shanxi, China

ARTICLE INFO

Keywords:
Cu diffusivity
Syngas
H_2S
DFT

ABSTRACT

Understanding the diffusion mechanism of Cu cluster over Cu surface is one of the important issues to predict and improve the stability of Cu-based catalyst. The diffusion of Cu adatom, Cu_2 and Cu_3 cluster over Cu(111) surface under different atmospheres (vacuum, CO, H_2 and H_2S atmosphere) at different temperatures have been investigated using density functional theory calculations. The results suggest that CO accelerates Cu surface diffusion at different temperatures, while H_2 atmosphere has little effect depending on the temperature. Further, under H_2S atmosphere, the negative formation energy of Cu-S complexes indicate that Cu-S species are more facile to form on Cu(111) surface. The diffusivity of CuS complex increases significantly with the decreasing of temperature and the increasing of H_2S concentration, which suggests that ppm H_2S results in the fast sintering of Cu surface significantly. This is consistent with the experimental result.

1. Introduction

Nowadays, much attention has been focused on the alcohol synthesis from syngas (CO + H_2), which has been regarded as one of the most promising technologies to provide the clean synthetic fuel [1,2]. The Cu-based catalysts are widely used for alcohol synthesis, such as methanol [3,4], ethanol [5,6], and even higher alcohols [7–9]. Meanwhile, great efforts have been devoted to establish the detailed structure-activity relationships of Cu-based catalysts in our and other groups [10–13]. However, Cu-based catalysts become deactivated easily during the operation owing to the sintering of Cu nanoparticles [14–18]. Therefore, improving the stability and understanding the sintering mechanism of Cu-based catalysts is also important.

Sintering corresponds to the process that the growth of catalyst particles starts from the smaller particles in heterogeneous catalysis, which is complicated and can be affected by not only the operating temperature but also the gas atmosphere [19–21]. In experiment, the catalyst deactivation rate is closely related to the gas-induced sintering [22–24]. The studies by Kuechen et al. [25] indicates that the deactivation rate strongly depends on the ratio of CO and CO_2 in the feed gas composition, and concludes that the presence of CO enhances the sintering of Cu particles by measuring the activity for 200–400 h over Cu catalyst. On the contrary, the deactivation rate of Cu-based catalyst increases in CO_2-rich feed rather than CO-rich feed during methanol synthesis due to the growth of Cu particle [26]. Sun et al. [27] found an accelerated deactivation by observing the activity of Cu catalyst for 50 h at 523 K as the mixed gas pressures of CO, CO_2 and H_2 increase.

On the other hand, it is well-known that sulfur-containing species significantly affect the catalyst stability in industrial syngas. For Cu-based catalyst, the sulfur-containing species can react readily with Cu metal surface, which slows down the rate of the reaction and deactivates the catalyst [28,29]. Importantly, only the trace amounts of sulfur will cause the catalyst deactivation. The deactivation mechanism is often attributed to the strong adsorption ability of sulfur [30,31], which occupies or affects the active site of catalyst. For example, trace amounts of S can occupy or affect small amounts of defect sites of Ni catalyst completely [32]. However, this mechanism cannot explain that why the trace amounts of S species can poison so much flat active sites on Cu catalyst. Therefore, the deactivation mechanism of Cu catalyst caused by S is still unclear. Further, much related studies have been carried out for solving the issue. Ling et al. [33] found that less than 0.01 monolayer of S can enhance surface self-diffusion by several orders of magnitude on Cu(111) surface, and the measured decay rate speedups with the increase of S coverage using low energy electron microscopy (LEEM) and scanning tunnel microscope (STM). Feibelman [34] and Walen et al. [35] attributed the promotion of surface sintering to Cu-S complex and supposed that Cu-S complex can enhance mass transport on Cu surface.

At present, there are the popular sintering mechanisms: (i) diffusion and coalescence, where clusters diffuse over the metal surface followed

* Corresponding author at: No. 79 Yingze West Street, Taiyuan 030024, China.
E-mail addresses: zhangriguang@tyut.edu.cn (R. Zhang), wangbaojun@tyut.edu.cn (B. Wang).

https://doi.org/10.1016/j.chemphys.2019.02.003
Received 7 July 2018; Received in revised form 17 January 2019; Accepted 7 February 2019
Available online 08 February 2019
0301-0104/

by coalescence [36]; (ii) ostwald ripening mechanism, where cluster emitted from one particle diffuses over the support (ZnO in Cu-based catalyst) and are captured by another particle [20]. Furthermore, the diffusion and coalescence mechanism on metal surface attracts more and more attentions [36,37]. In 1999, the studies of Horch et al. show that the mobility of Pt-H complex increases markedly on the clean Pt (110) surface and the bound H atom decreases the diffusion barrier compared to the Pt adatom alone using STM and density functional theory (DFT) calculations [38]. Subsequently, DFT studies by Shen et al. [39] indicate that the Ag-S complexes involving AgS_2, Ag_2S_2, Ag_2S_3, and Ag_3S_3 can potentially lead to the enhanced metal mass transport across the surface, and confirmed that trace amounts of S greatly enhance the coarsening of Ag adatom on Ag(111) surface. Recently, Nakao et al. [40] used DFT method to confirm that the formation of NiS complex affects the sintering behavior of Ni(111) depending on the temperature and the impurity H_2S concentration in the solid oxide fuel cell. More importantly, the calculated results explained well the experimental observation on Ni sintering under various temperatures and H_2S concentrations.

Nevertheless, as mentioned above, there are few theoretical studies about the effect of CO and H_2 atmosphere on Cu surface diffusion. More importantly, although the experiments show that the S-containing species can speedup surface Cu self-diffusion, there are few theoretical works to clarify the effect of the S-containing species. As a result, the effect of CO, H_2 and H_2S atmosphere on the surface Cu diffusion over Cu catalyst are investigated as a function of temperature using the density functional theory (DFT) calculations.

2. Computational details

2.1. Calculation methods and surface model

All calculations were performed by using the periodic DFT method implemented in Vienna Ab Initio Simulation Package (VASP) [41,42]. Projector-augmented wave (PAW) method was used for the core electrons and the generalized gradient approximation (GGA)-Perdew-Burke-Ernzerhof (PBE) formalism was used for the exchange correlation energy [43,44]. For the structure optimization, the wave functions were expanded in the plane-wave basis with the cutoff energy of 400 eV, and the electronic self-consistent cycle was converged to 5×10^{-6} eV, and the forces were smaller than 0.01 eV/Å. In addition, the vibrational frequency is analyzed using the same convergence criteria. And all the relaxed atoms in the structure optimization are analyzed. No imaginary frequencies are observed in the stable structures. The calculated zero-point energy (13.21 kJ·mol^{-1}) of CO molecule agrees well with the reported value (12.98 kJ·mol^{-1}) [45], which suggests the parameters for vibrational analysis are proper.

In order to locate the transition states for the diffusion of Cu species between the most stable and secondary stable sites on Cu(111) surfaces, the Climbing-Image Nudged Elastic Band method (CI-NEB) [46,47] was performed to obtain the minimum energy path between the most stable and secondary stable sites. The forces were less than 0.01 eV/Å. The transient state structure is confirmed with only one imaginary frequency.

The bulk structure of face-centered cubic Cu was optimized to obtain the lattice constant of 3.524 Å, which is close to the experimental value of 3.620 Å [48]. To model the diffusion of Cu species, four-layer Cu(111) slab surface with an vacuum thickness of 10 Å is constructed, in which the bottom layer was fixed, while the top three layers were relaxed. The size of surface slab was prepared by using $p(3 \times 3)$ and $p(6 \times 6)$. A $3 \times 3 \times 1$ k-point is used in all calculations. Further, to model the diffusion of Cu species, Cu clusters within three atoms have been considered. The size can reflect the diffusion process of Cu species sufficiently and the calculation cost is also acceptable [20,36,38–40,49].

2.2. Diffusivity

The diffusivity [50,51], D_M, (be also called the "mass transfer diffusivity"), is represented by the concentration C_{eq} and the intrinsic diffusivity D_I of diffusion species, normalized by the concentration of substrate atoms C_{sub}:

$$D_M = D_I \frac{C_{eq}}{C_{sub}} \tag{1}$$

where C_{eq} and C_{sub} are the concentration of diffusion species on substrate and substrate atoms, respectively; D_I is the intrinsic diffusivity of single diffusion species. The larger diffusivity D_M indicates the larger collision probability between diffusion species and promotes sintering of the catalyst. By the definition of D_M in Eq. (1), the diffusivity can decompose into two temperature-dependent factors for the diffusion species: one is the intrinsic diffusivity D_I, the other is the ratio of the equilibrium concentration $\frac{C_{eq}}{C_{sub}}$:

$$D_I = D_{0I} \exp(E_a/RT) \tag{2}$$

$$\frac{C_{eq}}{C_{sub}} = \exp(-\Delta G_{form}/RT) \tag{3}$$

where R is the gas constant, T is the absolute temperature, D_{0I} is the pre-exponential factor of diffusion, ΔG_{form} and E_a is the Gibbs formation energy of diffusion species and the activation energy of the diffusion, respectively. Then, the change of Gibbs formation energy is represented by the Eqs. (4) and (5):

$$\Delta G_{form} = G_{diff/surf} - G_{surf} - nG_{gas} - mG_{bulk} \tag{4}$$

$$G_{gas} = E_{gas} + G^c_{gas} = E_{gas} + [G_{gas}(T) + RT\ln(P/P^\theta)] \tag{5}$$

where $G_{diff/slab}$ is the Gibbs free energy of Cu surface with diffusion Cu species, G_{surf} is the Gibbs free energy of Cu surface, G_{gas} and G_{bulk} are the Gibbs free energy of the gas species and the atom in the bulk, respectively, and n and m represents the number of gas molecule and Cu atom within Cu species, respectively; G_{gas}(T) is the Gibbs free energy of the gas species at certain temperature T, P and P^θ represent the partial and standard partial, respectively. And the related data about the Gibbs free energy correction (G^c_{gas}) of the gas are presented in Table S3. In addition, note that we assume bulk state as the reference state of surface Cu species. The enthalpy and entropy terms were calculated from vibrational frequency to study the effect of the temperature on Gibbs free energy. The zero point vibrational energy was also considered. The smaller ΔG_{form}, the easier Cu species formed and the more Cu species exist on surface.

The pre-exponential factor D_{0I} [52] for single diffusion species is given by Eq. (6):

$$D_{0I} = \frac{n_p L^2}{2d} \frac{\prod_{i=1}^{3N} \nu_i}{\prod_{j=1}^{3N-1} \nu_j} \tag{6}$$

where n_p is the number of equivalent diffusion pathways, L is the diffusion distance, and d is the dimension of diffusion (in the case of surface diffusion, d equals to 2), ν_i and ν_j were vibrational frequencies at equilibrium and transition state structures, respectively.

3. Results and discussion

3.1. Diffusivity of Cu species under vacuum atmosphere

In order to evaluate the effect of gas atmosphere on Cu diffusion over Cu(111) surface, as a comparison, the diffusivity of Cu species under vacuum condition is firstly examined. Here, three kinds of Cu species are considered: Cu adatom, Cu_2 and Cu_3 clusters.

For Cu adatom, Cu_2 and Cu_3 clusters, the different adsorption structures at the top, bridge, fcc and hcp site on Cu(111) surface have

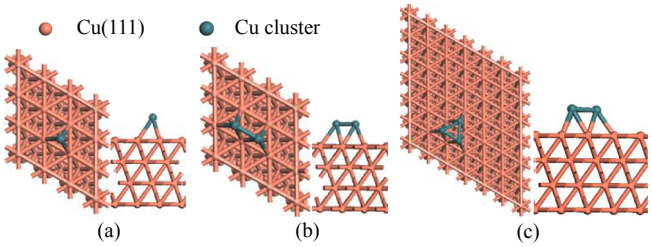

Fig. 1. The optimized structure for (a) Cu adatom, (b) Cu_2 cluster, and (c) Cu_3 cluster on Cu(111) surface.

Table 1
The formation free energy (E_{form}/kJ·mol^{-1}) of Cu adatom, Cu_2 cluster, and Cu_3 cluster at the fcc and hcp sites of Cu(111) surface at 0 K.

Clusters	The formation free energy	
	fcc	hcp
Cu adatom	87.51	88.19
Cu_2 cluster	150.42	152.06
Cu_3 cluster	160.72	160.61

been considered. The optimized structures and the corresponding formation free energy at 0 K are shown in Fig. 1 and Table 1, respectively. Seen from Table 1, the lowest formation energies of Cu and Cu_2 cluster are 87.51 and 150.42 kJ·mol^{-1}, respectively, which agree with the reported values by Rasmussen et al. [20] and Liu et al. [53] (77.19 kJ·mol^{-1} for Cu and 123.50 kJ·mol^{-1} for Cu_2). The formation energy of Cu_3 cluster are 160.61 and 160.72 kJ·mol^{-1} at the hcp and fcc site, respectively. The results show that the most stable sites of Cu adatom and Cu_2 cluster over Cu(111) surface are the fcc site, which agree well with the results by Liu et al. [53] and Rasmussen et al. [20], while Cu_3 cluster prefers to adsorb at both fcc and hcp site considering the similar formation energies. The secondary stable site is the bridge one. All Cu species initially adsorbed at the top site migrates to the three-fold site after geometry optimization. Thus, the diffusion of these Cu species may happen at the bridge site rather than that at the top site. Further, as shown in Table 1, Cu_2 and Cu_3 clusters are less stable by 62.91 and 73.23 kJ·mol^{-1} than Cu adatom, therefore, Cu adatom is more easier to form, namely, the most abundant species on Cu(111) surface at 0 K under vacuum condition.

For the effect of the temperature on the formation of Cu species, the temperature dependence of formation energy of Cu species was plotted, as shown in Fig. 2. As the temperature increases, the formation free

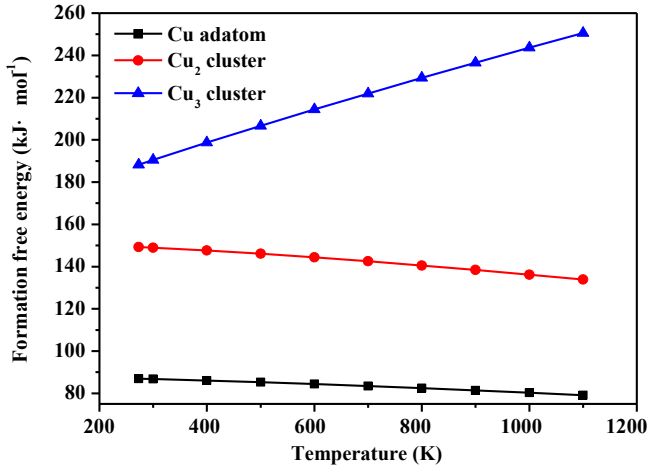

Fig. 2. The formation free energy of Cu adatom, Cu_2 and Cu_3 cluster on Cu(111) surface at different temperatures.

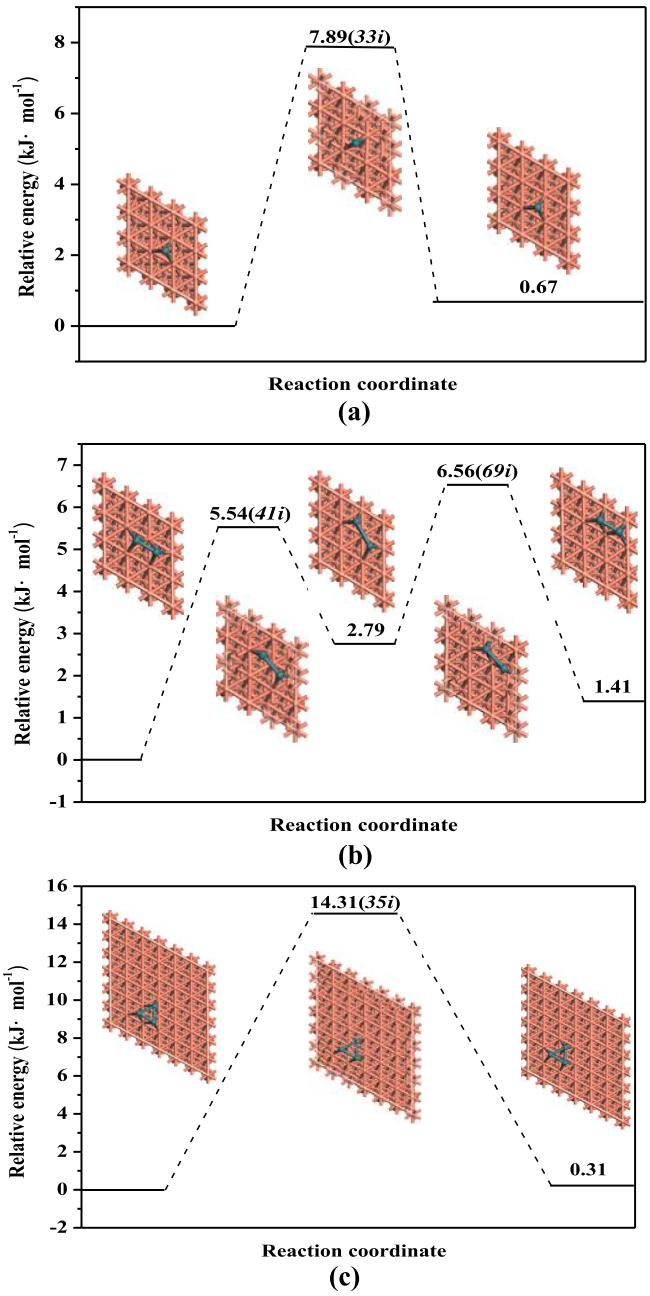

Fig. 3. The optimal energy path of surface diffusion for (a) Cu adatom, (b) Cu_2 cluster, and (c) Cu_3 cluster on Cu(111) surface together with the optimized structures of initial, transition, and final states. The imaginary frequencies (ν/cm^{-1}) are listed in the parentheses.

energy of Cu adatom and Cu_2 cluster became smaller slightly, while that of Cu_3 cluster became larger, which can be attributed to the increasing of the negative entropy change (see Fig. S1). The results indicate that as the temperature increases, the formation of Cu adatom and Cu_2 cluster become easier compared to that of Cu_3 cluster under the vacuum condition. Further, Cu adatom is the most abundant species over Cu(111) surface at the temperature range from 273 to 1100 K.

Furthermore, the diffusion paths of three Cu species between the most stable and the secondary stable site have been studied, and the optimal energy path and the configurations for diffusions of Cu adatom, Cu_2 and Cu_3 cluster are shown in Fig. 3. The diffusion path of Cu adatom is very simple, in which Cu adatom migrates from the three-fold fcc to hcp site via the bridge site with the activation barrier of 7.89 kJ·mol^{-1} on Cu(111) surface. The studies by Liu et al. [53] and

Rasmussen et al. [20] shows that the diffusion barrier of Cu on Cu(111) surface is below 10 kJ·mol^{-1}, which accords with the result (7.89 kJ·mol^{-1}). In the case of Cu_2 cluster, the path goes through two sequential transition states; one of two Cu atoms adsorbed at the fcc site firstly crosses the bridge site with the activation barrier of 5.54 kJ·mol^{-1}, then, it ends at the hcp site in the final state. Next, the other Cu atom also moves across the bridge site to a hcp site with an activation barrier of 3.77 kJ·mol^{-1}. In the other path that both Cu atoms move simultaneously from two fcc sites to two hcp sites via the bridge sites, the activation barrier is 10.65 kJ·mol^{-1}. Thus, Cu_2 cluster diffusion prefers to the former path with the overall activation barrier of 5.54 kJ·mol^{-1}, which is similar with the diffusion barrier of 5.40 kJ·mol^{-1} for Cu_2 cluster by Rasmussen et al. [20]. For the diffusion of Cu_3 cluster, three Cu atoms move simultaneously starting from the hcp sites over three bridge sites to end at the fcc sites with an activation barrier of 14.31 kJ·mol^{-1}.

For the effect of the temperature on surface diffusion of Cu species, the diffusivity of Cu adatom, Cu_2 and Cu_3 cluster are calculated by the formation free energy, activation barrier, and pre-exponential factor. The pre-exponential factors of Cu adatom, Cu_2 cluster, and Cu_3 cluster are 3.40×10^{-8}, 6.90×10^{-9}, and 2.45×10^{-9} m^2·s^{-1}, respectively. Fig. 4 presents the diffusivity of Cu species on Cu(111) surface under vacuum condition. As the temperature increases, the diffusivity of Cu adatom, Cu_2 cluster, and Cu_3 cluster becomes faster, and the diffusivity of Cu adatom and Cu_2 cluster are faster than that of Cu_3 cluster. Namely, Cu adatom and Cu_2 cluster are responsible for Cu diffusion, and the main diffusion Cu species depends on temperature on Cu(111) surface.

3.2. Diffusivity of Cu species under CO atmosphere

To evaluate the effect of CO atmosphere on the surface diffusion of Cu species, Cu-CO complexes including CuCO, Cu_2CO, $Cu_2(CO)_2$, Cu_3CO, $Cu_3(CO)_2$, and $Cu_3(CO)_3$ complex have been calculated. Fig. 5 and Table 2 summarize the optimized structures and formation free energy for each Cu-CO complex at 0 K.

Seen from Fig. 5, CO prefers to adsorb at the top site of Cu cluster. As shown in Table 2, $Cu_3(CO)_3$ complex is the most abundant complex with the lowest formation free energy of −146.66 kJ·mol^{-1} on Cu(111) surface at 0 K under CO atmosphere. Further, the optimal energy path for the diffusion of $Cu_3(CO)_3$ complex has been calculated to obtain the diffusivity. However, we observed that CO has the trend of the separation from Cu cluster in the diffusion process. Therefore, we further consider the diffusion of $Cu_2(CO)_2$ complex due to the lower formation energy (−66.45 kJ·mol^{-1}), which is the second lowest among all of Cu-CO complexes. In the structure of $Cu_2(CO)_2$ complex, two Cu atoms adsorb at the fcc site with two adsorbed CO molecules at the top site of Cu_2 cluster.

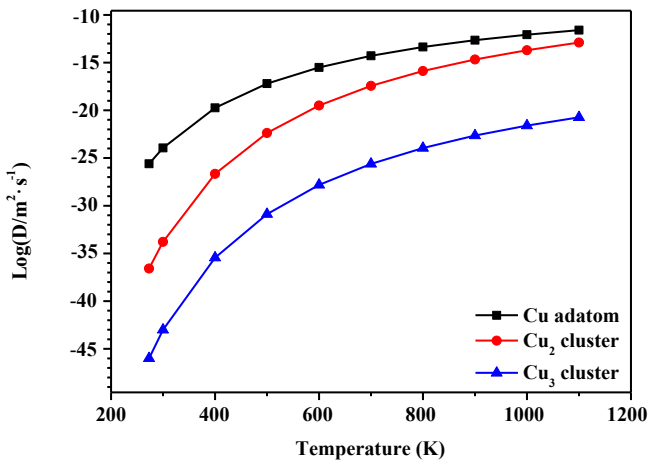

Fig. 4. The diffusivity of Cu adatom, Cu_2 and Cu_3 cluster on Cu(111) surface at different temperatures.

Then, the optimal energy path for the diffusion of $Cu_2(CO)_2$ complex from three-fold fcc to hcp sites via the bridge site on Cu(111) surface is shown in Fig. 6. The corresponding activation barrier and the pre-exponential factor is 17.29 kJ·mol^{-1} and 2.73×10^{-6} m^2·s^{-1}, respectively. Further, as shown in Fig. 7, as the temperature increases from 300 to 900 K, the diffusivity of $Cu_2(CO)_2$ complex decreases. However, the diffusivity of $Cu_2(CO)_2$ complex grows exponentially (from 10^2 to 10^5) as CO pressure increases from 0.5 to 12.5 atm (the assumption that Cu-CO complex on surface is an independent point without the mutual interaction under different CO pressure), and is larger obviously the diffusivity of Cu_2 cluster (10^{-40}–10^{-15}) under vacuum condition. Therefore, CO atmosphere significantly accelerates Cu surface diffusion at different temperatures, which accords well with the results by Kuechen et al. [25].

3.3. Diffusivity of Cu species under H_2 atmosphere

In order to evaluate the effect of H_2 atmosphere on the surface diffusion of Cu species and in view of the dissociative adsorption of H_2 molecule into the adsorbed H atoms on Cu surface [54], Cu-H complexes including CuH, Cu_2H, Cu_2H_2, Cu_3H, Cu_3H_2, and Cu_3H_3 complex under H_2 atmosphere have been calculated. Fig. 8 and Table 2 summarize the optimized structures and formation free energy for each Cu-H complex at 0 K.

Cu_2H_2 complex is the most abundant complex with the lowest formation free energy of 88.48 kJ·mol^{-1} on Cu(111) surface at 0 K. As shown in Fig. 8(b), two Cu atoms are adsorbed at the fcc site with one H atom seating at the bridge site and the other at the three-fold site. Further, the optimal energy path for the diffusion of Cu_2H_2 complex has been calculated to obtain the diffusivity. As shown in Fig. 9, both of Cu and H atoms are located at the bridge site in the transition state structure. The corresponding activation barrier and the pre-exponential factor is 9.81 kJ·mol^{-1} and 6.22×10^{-9} m^2·s^{-1}, respectively. Further, in order to conforms to gas composition ($P_{H2}/P_{CO} = 2$) in the syngas reaction, 1 and 25 atm are selected to study the diffusion of Cu species under different H_2 pressures. As shown in Fig. 10, compared to diffusivity of Cu_2 cluster under vacuum condition, the diffusivity of Cu_2H_2 complex slows down under different H_2 pressures at high temperature but increases at low temperature, which suggests the effect of H_2 atmosphere on Cu surface diffusion depends on the temperature. On the other hand, as the partial pressure of H_2 increases from 1 to 25 atm (the assumption that Cu-H complex on surface is an independent point without the mutual interaction under different H_2 pressure), there are slightly change for diffusivity of Cu_2H_2 complex, indicating that H_2 atmosphere has little effect on surface diffusion of Cu species over Cu (111) surface. Compared to Pt and Ni catalyst that hydrogen accelerates Pt and Ni surface diffusion [39,55,56], Cu catalyst performs the resistance of sintering caused by H_2 atmosphere.

3.4. Diffusivity of Cu species under H_2S atmosphere

Under H_2S atmosphere, we focus a system where there is a small amount of H_2S gas on Cu(111) surface, which does not lead to the formation of copper sulfide and isolated Cu adatom is negligible. Then, H_2S can potentially combine with Cu adatom from the step site to form Cu-S complex. Similarly, considering the dissociative adsorption of H_2S molecule on Cu surface [57], six Cu-S complexes involving CuS, Cu_2S, Cu_2S_2, Cu_3S, Cu_3S_2, and Cu_3S_3 complex have been considered. In addition, Cu_2S_3 complex, as observed by Walen et al. [35] using STM, is also considered in this study. Fig. 11 and Table 2 show the optimized structures and the formation free energy for each Cu-S complex at 0 K.

As listed in Table 2, the negative formation free energies of each Cu-S complex indicate that S atom is more facile bind to Cu species to form

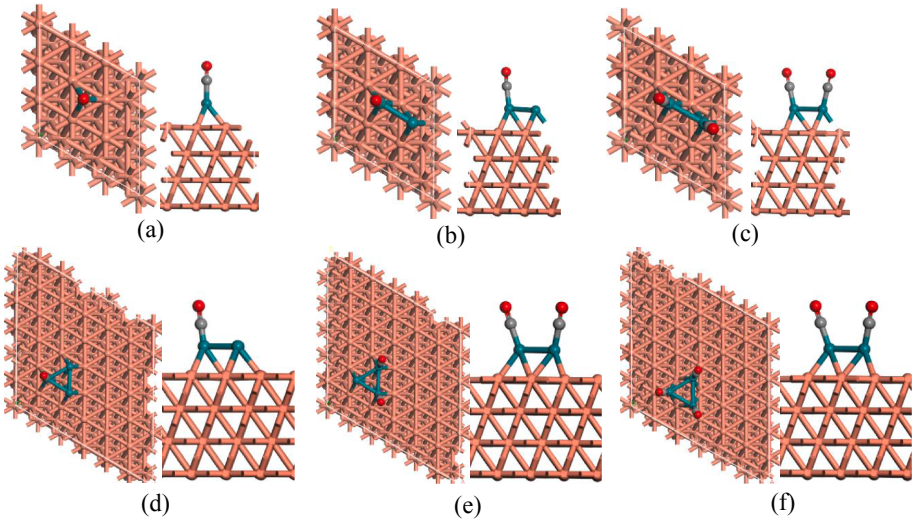

Fig. 5. The optimized structure for (a) CuCO, (b) Cu_2CO, (c) $Cu_2(CO)_2$, (d) Cu_3CO, (e) $Cu_3(CO)_2$, and (f) $Cu_3(CO)_3$ complexes on Cu(111) surface.

Table 2
The formation free energy (E_{form}/kJ·mol^{-1}) of different Cu-CO, Cu-H and Cu-S complexes over Cu(111) surface at 0 K under the corresponding CO, H_2, and H_2S atmosphere, respectively.

Cu-CO	E_{form}	Cu-H	E_{form}	Cu-S	E_{form}
CuCO	−24.54	CuH	92.92	CuS	−162.87
Cu_2CO	42.40	Cu_2H	110.19	Cu_2S	−117.90
$Cu_2(CO)_2$	−66.45	Cu_2H_2	88.48	Cu_2S_2	−399.14
Cu_3CO	59.47	Cu_3H	135.08	Cu_3S	−142.51
$Cu_3(CO)_2$	−44.12	Cu_3H_2	117.42	Cu_3S_2	−420.67
$Cu_3(CO)_3$	−147.06	Cu_3H_3	93.30	Cu_3S_3	−759.92
				Cu_2S_3	−775.97

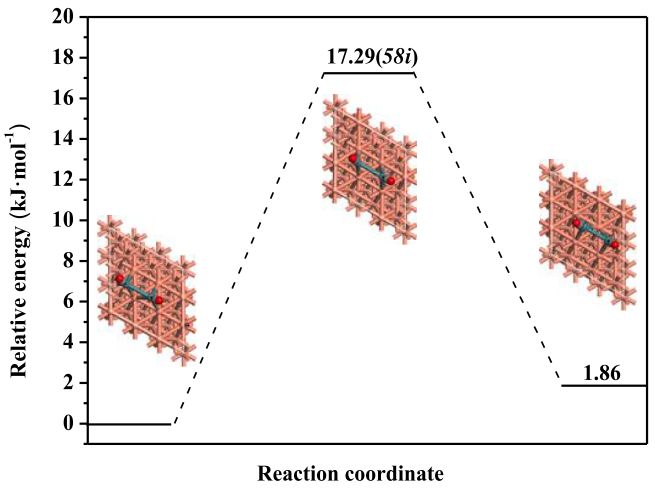

Fig. 6. The optimal energy path of surface diffusion for $Cu_2(CO)_2$ cluster on Cu (111) surface together with the optimized structures of initial, transition, and final states. The imaginary frequencies (ν/cm^{-1}) are listed in the parentheses.

the stable Cu-S complex than CO molecule and H atom. Further, as the number increasing of S atom in Cu-S cluster within the same size, the formation free energy becomes more negative, which suggest Cu-S cluster become more easily formed as the concentration of H_2S increases. Walen et al. [35], Feibelman [34] and Liu et al. [58] using DFT method also study the formation of Cu-S cluster on Cu(111) surface. Although the formation energies of Cu-S cluster in this study cannot be compared with those directly owing to the different references, the small formation energies [34,35,58] indicate the formation of Cu-S

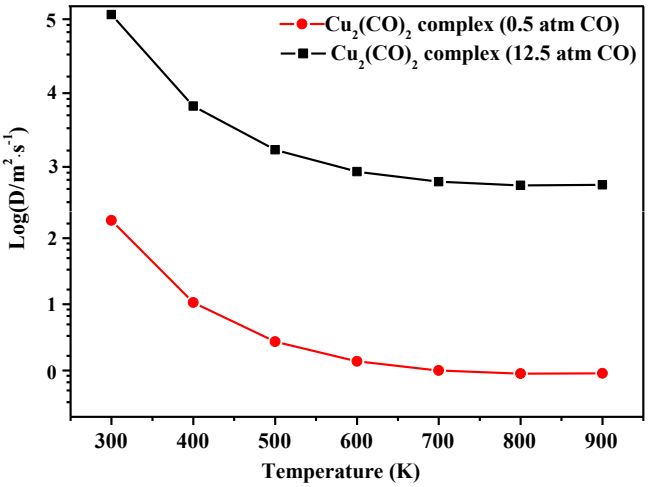

Fig. 7. The diffusivity of Cu-CO complex on Cu(111) surface with different CO partial pressures at different temperatures.

cluster is very facile, and especially, the formation energies of Cu-S cluster become smaller with the increasing number of S atom [35], which accords well with our results. Meanwhile, the adsorption of isolated S atom on Cu(111) surface is also calculated and the adsorption energy of −226.96 kJ·mol^{-1} indicates the strong interaction between S species and Cu metal, which can stabilize Cu-S complex and make Cu-S complex become the abundant surface diffusion species. Moreover, it can be found that Cu_2S_3 complex is the most abundant Cu-S species with the lowest formation free energy of −775.97 kJ·mol^{-1} on Cu(111) surface at 0 K under H_2S atmosphere, which confirm the experimental result [35]. However, considering the larger and stable Cu-S clusters can form from Cu adatom [59–61], as a result, we focused on the formation and diffusion of CuS complex to represent Cu-S complex.

As shown in Fig. 11(a), in the structure of CuS complex, Cu and S atom adsorb at the opposite fcc and hcp site, respectively. The formation free energy is −162.87 kJ·mol^{-1}. Further, based on these calculated results, the optimal energy path for the diffusion of CuS complex has been calculated. As shown in Fig. 12, in the initial state, Cu and S atom adsorb at the fcc and the opposite hcp site, respectively; then, CuS complex moves simultaneously to the nearest three-fold sites via the transition state, in which Cu and S atoms adsorb at the bridge and the diagonal top site, respectively. The corresponding activation barrier and pre-exponential factor of CuS complex is 51.01 kJ·mol^{-1} and

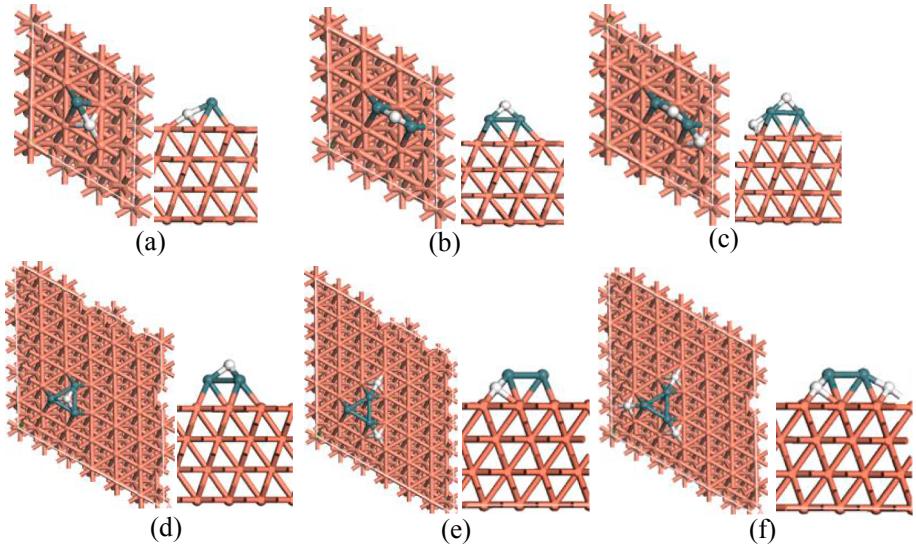

Fig. 8. The optimized structure for (a) CuH, (b) Cu_2H, (c) Cu_2H_2, (d) Cu_3H, (e) Cu_3H_2, and (f) Cu_3H_3 complexes on Cu(111) surface.

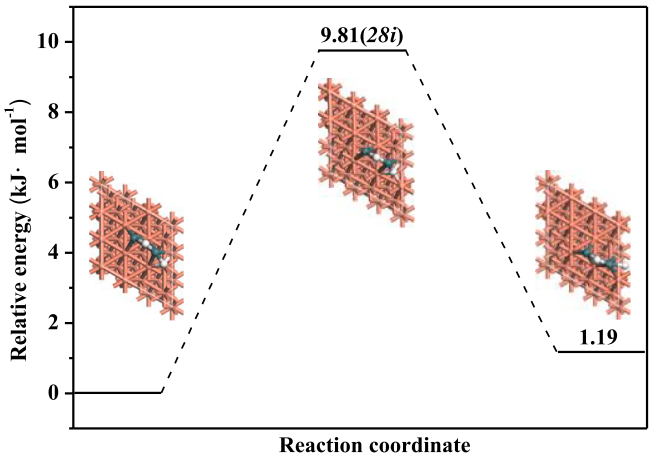

Fig. 9. The optimal energy path of surface diffusion for Cu_2H_2 cluster on Cu (111) surface together with the optimized structures of initial, transition, and final states. The imaginary frequencies (ν/cm^{-1}) are listed in the parentheses.

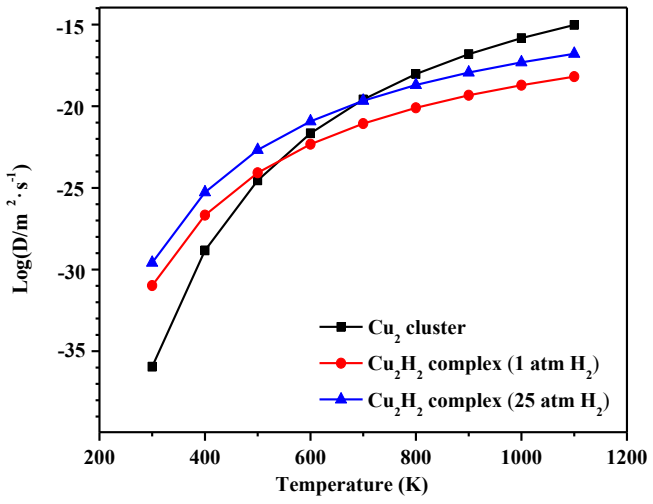

Fig. 10. The diffusivity of Cu-H complex on Cu(111) surface with different H_2 partial pressures at different temperatures.

6.57×10^{-8} m^2·s^{-1}, respectively.

Further, considering the ppm level of S poisons Cu catalyst, the surface diffusivities of CuS complex under 0.1, 1 and 10 ppm H_2S have been shown in Fig. 13. The diffusivity of CuS complex under different H_2S concentrations is far higher than that of Cu adatom under vacuum condition and increases rapidly as the temperature decreases from 1100 to 800 K, suggesting the addition of sulfur accelerates surface diffusion of Cu species. The increasing surface diffusion of Cu species further leads to the aggregation and sintering of Cu surface under H_2S atmosphere, which are in keeping with other studies [34,35,58]. Therefore, the S-containing species can accelerate the sintering of Cu surface. On the other hand, as the H_2S concentration increases from 0.1 to 10 ppm, the diffusivity of CuS complex becomes faster, suggesting that Cu surface is extremely sensitive to the S-containing impurities, and performs lower sulfur tolerance with only ppm levels.

Experimentally, Chai et al. [62] observed the different levels of deactivation for the Cu-based catalysts after pulsing 0.5–1.0 ppm H_2S in the methanol synthesis, which reveals that Cu-based catalyst has lower sulfur tolerance and could be sensitive to the S-containing impurities. Ma et al. [63] measured CO conversion within 3 ppm H_2S for methanol synthesis from syngas over the Cu catalyst at 513 K, indicating that CO conversion decreases from 24.5% to lower than 1%, and the catalyst deactivates sharply under the S-containing species atmosphere. Beale et al. [64] also use chemical imaging methods to find that the higher the H_2S concentration is, the greater the extent of deactivation of Cu catalyst is. Our results can provide a reasonable interpretation for the deactivation observed in experiment indirectly. In addition, the copper sulfide phase may form under the higher H_2S concentration, for example, Ma et al. [63] observed the copper sulfide phase under the atmosphere of 30 ppm of H_2S. However, the formation of copper sulfide phase is beyond our research in this study. And it might be necessary to understand the formation of copper sulfide phase in the future work.

4. Conclusions

In this study, the diffusivity of Cu species on Cu(111) surface under vacuum atmosphere, as well as CO, H_2 and H_2S atmosphere have been examined using DFT calculations. Under vacuum condition, the diffusivity of Cu adatom, Cu_2 cluster, and Cu_3 cluster become faster with the increasing of the temperature. However, the diffusivity of Cu adatom and Cu_2 cluster are faster than that of Cu_3 cluster at different temperatures, which indicates that Cu adatom and Cu_2 cluster are responsible for Cu transport on Cu(111) surface. Under CO atmosphere,

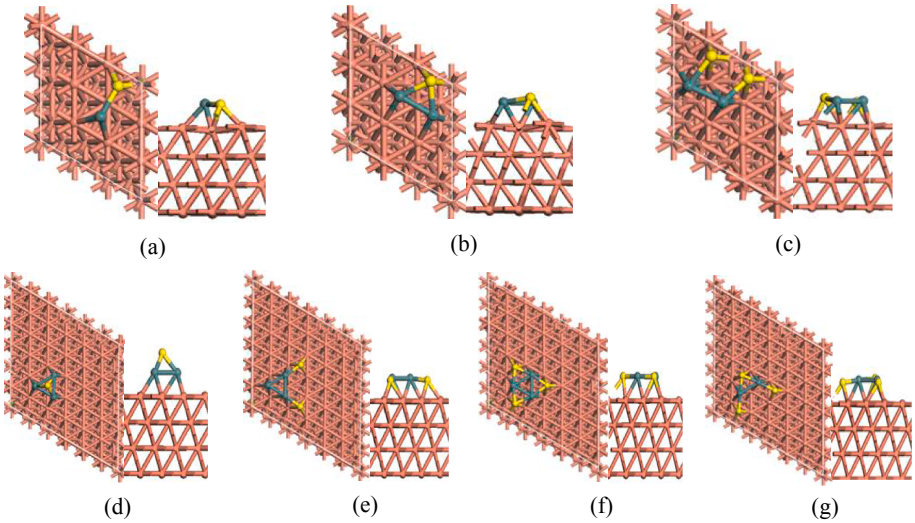

Fig. 11. The optimized structure for (a) CuS, (b) Cu_2S, (c) Cu_2S_2, (d) Cu_3S, (e) Cu_3S_2, (f) Cu_3S_3 and (g) Cu_2S_3 complexes on Cu(111) surface.

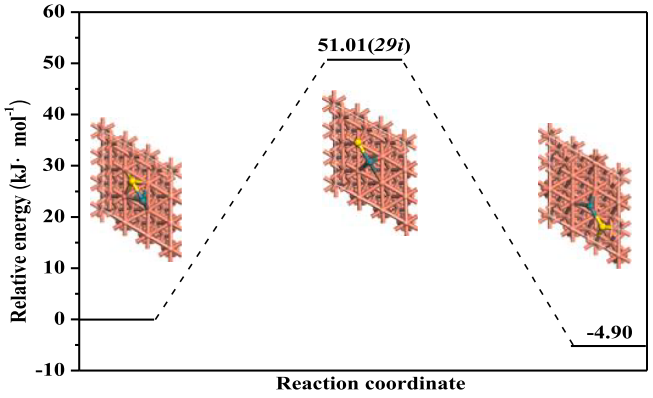

Fig. 12. The optimal energy path of surface diffusion for CuS complex on Cu (111) surface together with the optimized structures of initial, transition, and final states. The imaginary frequencies (ν/cm^{-1}) are listed in the parentheses.

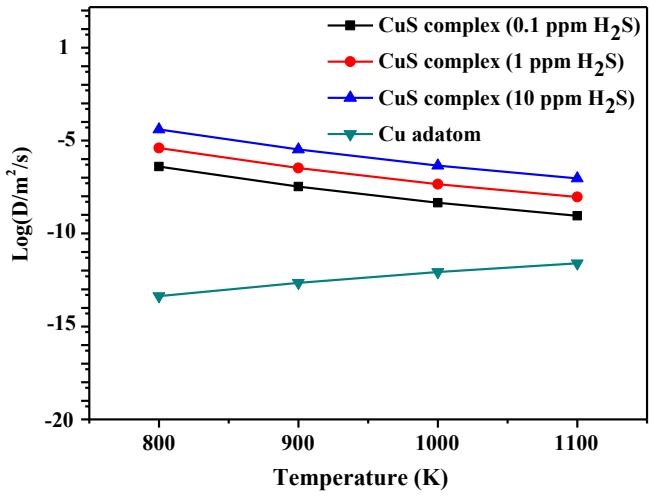

Fig. 13. The diffusivity of Cu-S complex on Cu(111) surface with different H_2S concentrations at different temperatures.

as the CO pressure increases and the temperature decreases, the diffusivity of $Cu_2(CO)_2$ complex increases and is larger than the diffusivity of Cu_2 cluster, suggesting CO atmosphere can accelerate Cu surface diffusion significantly. Under H_2 atmosphere, the diffusivity of Cu_2H_2 complex change slightly as H_2 pressure increases, the main diffusion species is Cu_2H_2 complex at low temperature while Cu_2 cluster at the high temperature, suggesting that the effect of H_2 atmosphere on Cu surface diffusion is weak and depends on the temperature.

For the impurity H_2S in feed gas, the negative formation free energies indicate that Cu-S complexes are easy to form on Cu(111) surface. Ppm H_2S accelerates the diffusivity of CuS complex significantly within the decreasing of temperature and the increasing of H_2S concentration. Therefore, Cu surface is extremely sensitive to the S-containing species, and performs lower sulfur tolerance, which agrees well with the experimental results. Importantly, the study gives out the microscopic mechanism at the molecular level that why only ppm levels H_2S leads to the sintering of Cu surface, the complete removal of S-containing impurities in the feed gas is necessary to prevent the sinter of Cu surface considering the high sensitivity to sulfur on Cu-based catalysts.

Acknowledgment

This work is financially supported by the Key Projects of National Natural Science Foundation of China (21736007), the National Natural Science Foundation of China (No. 21776193, 21476155), the Program for the Top Young Academic Leaders of Higher Learning Institutions of Shanxi, the Top Young Innovative Talents of Shanxi.

Appendix A. Supplementary data

Supplementary data to this article can be found online at https://doi.org/10.1016/j.chemphys.2019.02.003.

References

[1] P.L. Spath, D.C. Dayton, National Renewable Energy Laboratory Press: Golden, Colorado, USA, 2003.
[2] V.R. Surisetty, A.K. Dalai, J. Kozinski, Appl. Catal. A: Gen. 404 (2011) 1–11.
[3] W.R.A.M. Robinson, J.C. Mol, Appl. Catal. 60 (1990) 73–86.
[4] M. Behrens, F. Studt, I. Kasatkin, S. Kühl, M. Hävecker, F. Abild-Pedersen, S. Zander, F. Girgsdies, P. Kurr, B.L. Kniep, M. Tovar, R.W. Fischer, J.K. Nørskov, R. Schlögl, Science 336 (2012) 893–897.
[5] J.L. Gong, H.R. Yue, Y.J. Zhao, S. Zhao, L. Zhao, J. Lv, S.P. Wang, J. Am. Chem. Soc. 134 (2012) 13922–13925.
[6] M. Gupta, M.L. Smith, J.J. Spivey, ACS Catal. 1 (2011) 641–656.
[7] J.G. Nunan, C.E. Bogdan, K. Klier, K.J. Smith, C.W. Young, R.G. Herman, J. Catal. 116 (1989) 195–221.
[8] G. Prieto, S. Beijer, M.L. Smith, M. He, Y. Au, Z. Wang, D.A. Bruce, P.K. De Jong, J.J. Spivey, P.E. De Jongh, Angew. Chem. Int. Ed. 53 (2014) 6397–6401.
[9] Y.W. Lv, B.B. Cao, F. Yu, J. Liu, Z.H. Bao, J.S. Gao, Chem. Catal. Chem. 6 (2014) 473–478.
[10] R.G. Zhang, G.R. Wang, B.J. Wang, L.X. Ling, J. Phys. Chem. C 118 (2014)

5243–5254.
[11] R.G. Zhang, X.C. Sun, B.J. Wang, J. Phys. Chem. C 117 (2013) 6594–6606.
[12] G.C. Wang, L. Jiang, Z.S. Cai, Y.M. Pan, X.Z. Zhao, W. Huang, K.C. Xie, Y.W. Li, Y.H. Sun, B. Zhong, J. Phys. Chem. B 107 (2003) 557–562.
[13] H.Y. Zheng, R.G. Zhang, Z. Li, B.J. Wang, J. Mol. Catal. A: Chem 404 (405) (2015) 115–130.
[14] J.C.J. Bart, R.P.A. Sneeden, Catal. Today 2 (1987) 1–124.
[15] G.C. Chinchen, P.J. Denny, J.R. Jennings, M.S. Spencer, K.C. Waugh, Appl. Catal. 36 (1988) 1–65.
[16] M.V. Twigg, M.S. Spencer, K. Mansfield, Top. Catal. 22 (1990) 191–203.
[17] R. Hughes, Academic Press: New York, 1984.
[18] G. Tammann, Leopold Voss Press: Leipzig, 1923.
[19] C.T. Campbell, S.C. Parker, D.E. Starr, Science 298 (2002) 811–814.
[20] D.B. Rasmussen, T.V.W. Janssens, B. Temel, T. Bligaard, B. Hinnemann, S. Helveg, J. Sehested, J. Catal. 293 (2012) 205–214.
[21] Y. Bai, J. Zhang, G. Yang, Q. Zhang, J. Pan, H. Xie, X. Liu, Y. Han, Y. Tan, ACS Catal. 8 (2018) 6367–6374.
[22] J.A. Moulijn, A.E. van Diepen, F. Kapteijn, Appl. Catal. A: Gen, 212 (2001) 3–16.
[23] P.J.F. Harris, Inorg. Chem. 40 (1995) 97–115.
[24] P. Wynblatt, N.A. Gjostein, Prog. Solid State Chem. 9 (1975) 21–58.
[25] C. Kuechen, U. Hoffmann, Chem. Eng. Sci. 48 (1993) 3767–3776.
[26] J.G. Wu, M. Saito, M. Takeuchi, T. Watanabe, Appl. Catal. A: Gen. 218 (2001) 235–240.
[27] J.T. Sun, I.S. Metcalfe, M. Sahibzada, Ind. Eng. Chem. Res. 38 (1999) 3868–3872.
[28] Q. Wang, J.H. Zhu, S.Y. Wei, J.S. Chung, Z.H. Guo, Ind. Eng. Chem. Res. 49 (2010) 7330–7335.
[29] J. Liu, X.Y. Li, Q.D. Zhao, C. Hao, S.B. Wang, M. Tade, ACS Catal. 4 (2014) 2426–2436.
[30] M. Foss, R. Feidenhans'l, M. Nielsen, E. Findeisen, R.L. Johnson, T. Buslaps, I. Stensgaard, F. Besenbacher, Phys. Rev. B 50 (1994) 8950–8953.
[31] M. Foss, R. Feidenhans'l, M. Nielsen, E. Findeisen, T. Buslaps, R.L. Johnson, F. Besenbacher, Surf. Sci. 388 (1997) 5–14.
[32] B. Legras, V.V. Ordomsky, C. Dujardin, M. Virginie, A.Y. Khodakov, ACS Catal. 4 (2014) 2785–2791.
[33] W.L. Ling, N.C. Bartelt, K. Pohl, J.D.L. Figuera, R.Q. Hwang, K.F. McCarty, Phys. Rev. Lett. 93 (2004) 166101-1–4.
[34] P.J. Feibelman, Phys. Rev. Lett. 85 (2000) 606-1-9.
[35] H. Walen, D.J. Liu, J. Oh, H. Lim, J.W. Evans, C.M. Aikens, Y. Kim, P.A. Thiel, Phys. Rev. B 91 (2015) 045426-1–7.
[36] J. Sehested, J.A.P. Gelten, I.N. Remediakis, H. Bengaard, J.K. Nørskov, J. Catal. 223 (2004) 432–443.
[37] F.B. Rasmussen, J. Sehested, H.T. Teunissen, A.M. Molenbroek, B.S. Clausen, Appl. Catal. A: Gen. 267 (2004) 165–173.
[38] S. Horch, H.T. Lorensen, S. Helveg, E. Laegsgaard, I. Stensgaard, K.W. Jacobsen, J.K. Nùrskov, F. Besenbacher, Nature 398 (1999) 134–136.
[39] M.M. Shen, D.J. Liu, C.J. Jenks, P.A. Thiel, J.W.J. Evans, Chem. Phys. 130 (2009) 094701-1–13.
[40] N. Kazuhide, I. Takayoshi, K. Michihisa, J. Phys. Chem. C 120 (2016) 16641–16648.
[41] G. Kresse, J. Furthmüller, Phys. Rev. B: Condens. Matter 54 (1996) 11169–11186.
[42] G. Kresse, J. Furthmüller, Comput. Mater. Sci. 6 (1996) 15–50.
[43] J.P. Perdew, K. Burke, M. Ernzerhof, Phys. Rev. Lett. 77 (1996) 3865–3868.
[44] J.A. White, D.M. Bird, Phys. Rev. B: Condens. Matter 50 (1994) 4954–4957.
[45] X.C. Fu, W.X. Shen, T.Y Yao, Higher Education, Beijing, 1990.
[46] D. Sheppard, P. Xiao, W. Chemelewski, D.D. Johnson, G. Henkelman, J. Chem. Phys. 136 (2012) 074103-1–8.
[47] D. Sheppard, T. Rye, G. Henkelman, J. Chem. Phys. 128 (2008) 134106-1–10.
[48] L. Grabow, M. Mavrikakis, ACS Catal. 1 (2011) 365–384.
[49] J. Sehested, J. Catal. 217 (2003) 417–426.
[50] A.S. Dalton, E.G. Seebauer, Surf. Sci. 601 (2007) 728–734.
[51] E.G. Seebauer, C.E. Allen, Prog. Surf. Sci. 49 (1995) 265–330.
[52] G.H. Vineyard, J. Phys. Chem. Solid 3 (1957) 121–127.
[53] D.J. Liu, Phys. Rev. B 81 (2010) 035415-1–10.
[54] H.A. Michelsen, D.J. Auerbach, J. Chem. Phys. 94 (1991) 7502–7520.
[55] B. Mills, P. Douglas, G.M. Leak, Trans. Metall. Soc. AIME 245 (1969) 1291–1296.
[56] N. Azzerri, R.L. Colombo, Metallography 9 (1976) 233–244.
[57] P.N. Abufager, P.G. Lustemberg, C. Crespos, H.F. Busnengo, Langmuir 24 (2008) 14022–14026.
[58] D.J. Liu, J. Lee, T.L. Windus, P.A. Thiel, J.W. Evans, Surf. Sci. 676 (2018) 2–8.
[59] L. Ruan, I. Stensgaard, F. Besenbacher, E. Lægsgaard, Ultramicroscopy 42–44 (1992) 498–504.
[60] G. Ehrlich, F.G. Hudda, J. Chem. Phys. 44 (1966) 1039–1049.
[61] M. Breeman, D.O. Boerma, Surf. Sci. 269–270 (1992) 224–228.
[62] G. Chai, D. Ai, C. Li, Stud. Surf. Sci. Catal. 68 (1991) 539–547.
[63] Y.C. Ma, Q.J. Ge, W.Z. Li, H.Y. Xu, Catal. Commun. 10 (2008) 6–10.
[64] A.M. Beale, E.K. Gibson, M.G. O'Brien, S.D.M. Jacques, R.J. Cernik, M.D. Michiel, P.D. Cobden, P.G. Özlem, L. van de Water, M.J. Watson, B.M. Weckhuysen, J. Catal. 314 (2014) 94–100.